Harnessing an emissive guanine surrogate to design small-molecule fluorescent chemosensors of O6-methylguanine-DNA-methyltransferase (MGMT)

Alexandra Fillion, Jaime Franco Pinto, Anton Granzhan

COMMUNICATION

Harnessing an emissive guanine surrogate to design small-molecule fluorescent chemosensors of O^6-methylguanine-DNA-methyltransferase (MGMT)†

Received 00th January 20xx,
Accepted 00th January 20xx

DOI: 10.1039/x0xx00000x

Alexandra Fillion,[# a,b] Jaime Franco Pinto [# a,b] and Anton Granzhan *[a,b]

Fluorescence properties of an emissive guanine surrogate, thienoguanine ($^{th}G_N$, 2-aminothieno[3,4-*d*]pyrimidin-4(3*H*)-one), were exploited to design two real-time chemosensors of O^6-methylguanine-DNA-methyltransferase (MGMT), key DNA repair enzyme involved in the resistance to DNA-alkylating anti-cancer drugs though direct reversal of O^6-alkylated guanine adducts.

Temozolomide and Carmustine, two DNA-alkylating drugs approved for glioblastoma treatment, exert their cytotoxic effect chiefly by alkylating O6 atoms of guanine bases in DNA, producing adducts that trigger a futile mismatch repair process leading to replication fork stalling and cell death. Nonetheless, O^6-methylguanine-DNA-methyltransferase (MGMT, also known as AGT) removes alkyl residues from O^6-alkylated guanines through an irreversible S_N2 reaction with the cysteine residue of the enzyme, leading to deactivation of the enzyme and direct repair of the alkylated DNA, thereby alleviating the effect of anti-tumour treatment and leading to chemoresistance.[1–3] MGMT status of the tumour is crucial for assessing the prognosis and the choice of optimal treatment regime, since low MGMT expression is significantly associated with better treatment response and patient survival; conversely, administration of TMZ to patients with MGMT-positive glioblastoma leads to adverse drug effects reducing their quality of life without a therapeutic benefit.[4,5] Since promoter methylation is a major mechanism of gene silencing, methylation of the *MGMT* promoter, easily accessible through molecular biology techniques such as (quantitative) methylation-specific PCR (MSP and qMSP), bisulfite sequencing (BiSEQ), or pyrosequencing, emerged as a clinically used biomarker of the MGMT of tumours.[6] However, discordances between the *MGMT* promoter methylation status, actual MGMT expression levels and activity, and treatment outcomes have been highlighted in the literature.[5,7,8] Possible sources of these discrepancies include the strongly variable CpG methylation pattern of the promoter, methylation of the gene body and exons that equally affect *MGMT* expression, post-transcriptional regulation by miRNAs, and others.[5,9–11] In addition, both MGMT expression and activity were observed to increase in response to TMZ treatment independently of the promoter methylation status that remains stable during disease progression.[5] In this context, the development of robust, easy-to-implement methods to directly assess MGMT activity in tumour samples or cell cultures represents an urgent task.

Fluorescence-based diagnostic tools often represent a method of choice due to the high sensitivity and specificity of fluorogenic probes. Along these lines, profluorescent MGMT substrate analogues, namely oligonucleotides harboring O^6-substituted guanine derivatives endowed with a fluorophore[12] or a quencher[13] in the side chain, along with a FRET partner, have been exploited to construct fluorogenic chemosensors of MGMT activity. In this design, the reaction of the probe with MGMT leads to a transfer of the O^6-substituent from the substrate to the protein, leading to disruption of the FRET pair and an increase of fluorescence signal.[12,13] Alternatively, MGMT-promoted dealkylation of O^6-alkylated oligonucleotide substrates can be exploited to trigger a conformation switch, leading to a change of a fluorescence signal[14,15] or activation of a DNAzyme cleaving a fluorogenic RNA substrate.[16] However, a common drawback of oligonucleotide-based probes is their poor cellular permeability, making their use in live cells problematic. Finally, probes based on an MGMT pseudosubstrate O^6-benzylguanine (BG) conjugated to an external fluorophore[17–20] or a fluorophore–quencher pair,[21,22] that were originally designed for SNAP-tag protein labelling, can be exploited for labelling and detection of cellular MGMT. However, as the reaction of native MGMT with BG is slow, these probes require long reaction time for fluorophore transfer.[20]

While natural nucleosides are essentially non-fluorescent, the last decade witnessed a rise of fluorescent nucleoside analogues that found numerous applications in probing the

[a] *CNRS UMR9187, Inserm U1196, Institut Curie, PSL Research University, 91405 Orsay, France. E-mail: anton.granzhan@curie.fr*
[b] *CNRS UMR9187, Inserm U1196, Université Paris Saclay, 91405 Orsay, France.*
[#] These authors contributed equally to this work.
†Electronic Supplementary Information (ESI) available. See DOI: 10.1039/x0xx00000x

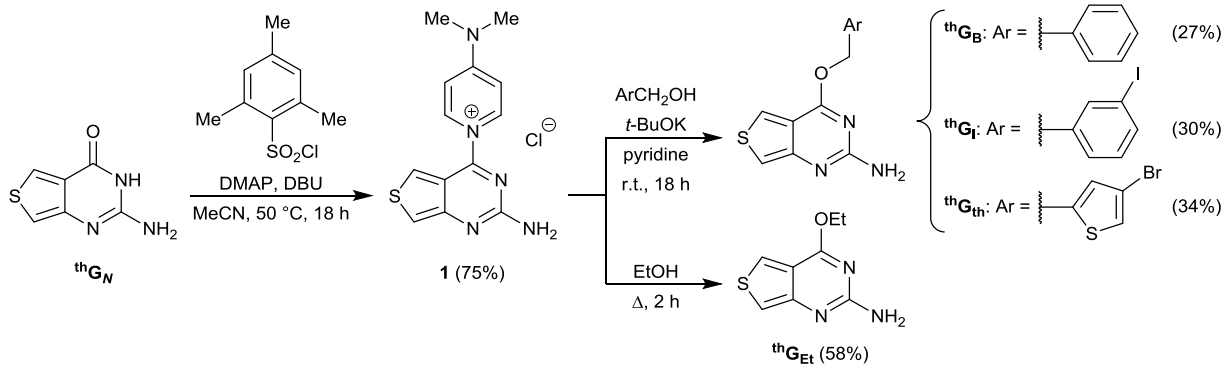

Scheme 1 Synthesis of chemosensors ($^{th}G_B$, $^{th}G_I$, $^{th}G_{th}$, and $^{th}G_{Et}$).

structure and dynamics of nucleic acids.[23,24] Among these, thienoguanosine (^{th}G), developed by Y. Tor et al.,[25] represents an easily accessible, highly emissive surrogate of guanosine that almost perfectly mimics the latter in nucleic acids, making it an outstanding fluorescent DNA probe.[26,27] In this work, we harnessed fluorescence properties of the corresponding nucleobase surrogate, thienoguanine ($^{th}G_N$, Scheme 1),[28] to design the smallest fluorescent chemosensors of MGMT activity.

The synthesis of O^6-substituted thienoguanine derivatives is shown on Scheme 1. Initial attempts to alkylate $^{th}G_N$ using benzyl alcohol in Mitsunobu conditions (PPh_3, DIAD, THF or dioxane) gave the desired compound $^{th}G_B$ in low yield (*ca.* 5%) along with undesired products of N1 and N3 alkylation; therefore, an alternative strategy was developed using the activated 4-(dimethylamino)pyridinium salt **1** that was obtained through a reaction of $^{th}G_N$ with a slight excess of DMAP in the presence of 2-mesitylenesulfonyl chloride and DBU in a good yield (75%). A similar strategy was previously employed for the synthesis of O^6-substituted guanine derivatives.[29] Salt **1** was made to react with benzyl, 3-iodobenzyl, or 4-bromothenyl alcohols in pyridine in the presence of a base (*t*-BuOK), to give O^6-alkylated derivatives ($^{th}G_B$, $^{th}G_I$, and $^{th}G_{th}$, respectively) in moderate yields (about 30%); in addition, refluxing the salt **1** in EtOH gave the O^6-ethyl derivative $^{th}G_{Et}$ in a 58% yield.

The basic photophysical properties of the probes are summarized in Table 1. The absorption spectra of all O^6-substituted derivatives were red-shifted by about 20 nm, and emission spectra by 10–13 nm, comparing with $^{th}G_N$ (Fig. 1). Importantly, the 400-nm shoulder in the emission spectrum of $^{th}G_N$, that was previously assigned to the H3 keto-amino tautomer,[30] was totally absent in the emission spectra of the derivatives (Fig. 1b), demonstrating that O^6 substitution blocks

Table 1 Photophysical data for O^6-substituted $^{th}G_N$ derivatives in water.[a]

Compound	$\lambda_{abs,max}$ / nm	ε / cm^{-1} M^{-1}	$\lambda_{em,max}$ / nm[b]	Φ[c]
$^{th}G_N$	315	3100	436	0.59[d]
$^{th}G_B$	337	3140	448	0.47
$^{th}G_I$	339	3240	449	0.28
$^{th}G_{th}$	338	2720	446	0.11
$^{th}G_{Et}$	332	3540	448	0.13

[a] c = 50 µM for absorbance, 5 µM for fluorescence measurements. [b] λ_{ex} = 325 nm. [c] Fluorescence quantum yield, reference: quinine sulphate in 0.5 M H_2SO_4 (Φ = 0.546). [c] This value is higher than the one reported in the literature (0.46),[25] presumably due to the use of another quantum yield standard.

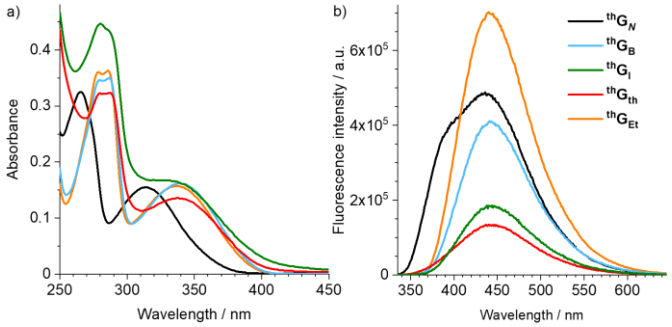

Fig. 1 a) Absorption (c = 50 µM) and b) emission (c = 5 µM, λ_{ex} = 325 nm) spectra of $^{th}G_N$ and its O^6-substituted derivatives in water.

the formation of this tautomer. The fluorescence quantum yield of $^{th}G_{Et}$ was only slightly lower, and that of $^{th}G_B$ was about two times lower than the one of $^{th}G_N$. However, the fluorescence of both $^{th}G_I$ and $^{th}G_{th}$ was decreased about 5-fold comparing with $^{th}G_N$, giving evidence of the quenching effect of heavy-atom substituents in the O^6-arylmethyl group (I and Br, respectively) on the fluorescence of the thienoguanine core. These two "dark" derivatives could be considered as promising MGMT chemosensors, as their reaction with the enzyme would lead to a transfer of the arylmethyl group to the enzyme and a release of the highly emissive $^{th}G_N$ (Fig. 2a).

The reaction of $^{th}G_{th}$ and $^{th}G_I$ with MGMT was assessed by monitoring real-time changes of fluorescence intensity of the probes (100 nM) in the presence of varied concentrations of the enzyme. While the fluorescence of both probes, monitored at 400 nm, remained low in the absence of the enzyme, addition of MGMT led to a rapid increase of fluorescence

reaching a plateau whose level was dependent on the amount of added MGMT, giving evidence of a stoichiometric reaction (Fig. 2b, c). In the presence of slight excess of the enzyme (1.4 molar equiv.), the level of the plateau almost matched the fluorescence intensity of the equimolar $^{th}\mathbf{G}_N$ solution, indicating complete conversion of the probe in both cases. To assess the kinetics of enzymatic dealkylation, the reaction was performed in the conditions of an excess of the probe with respect to the enzyme (5 molar equiv.). In these conditions, the reaction follows a pseudo-first-order kinetics with apparent rate constants k_{app} = 0.00172 and 0.00534 s^{-1} for $^{th}\mathbf{G}_I$ and $^{th}\mathbf{G}_{th}$ ($\tau_{½}$ = 400 and 130 s, respectively), indicating that $^{th}\mathbf{G}_{th}$ is a 3.1-fold faster MGMT probe than $^{th}\mathbf{G}_I$ (Fig. S1, ESI†). This is in agreement

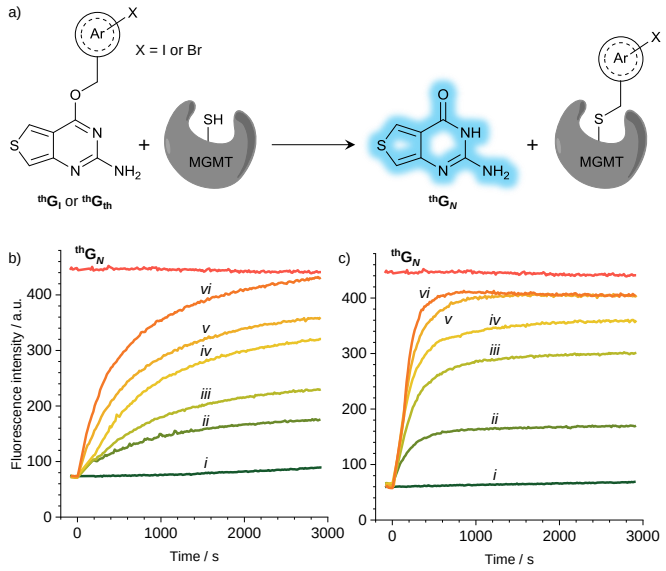

Fig. 2 a) Scheme of MGMT-promoted dealkylation of chemosensors leading to formation of the emissive $^{th}\mathbf{G}_N$. b–c) Real-time fluorescence changes of b) $^{th}\mathbf{G}_I$ and c) $^{th}\mathbf{G}_{th}$ in the absence (*i*) and in the presence (*ii*–*vi*) of increasing amounts of MGMT (final concentration, *ii*: 23 nM, *iii*: 48 nM, *iv*: 68 nM, *v*: 95 nM, *vi*: 144 nM) added at t = 0. Conditions: c(probe) = 100 nM in the reaction buffer (10 mM Tris-HCl, 100 mM NaCl, 1 mM DTT, 5% v/v DMSO, pH 8.5), λ_{ex} = 314 nm, λ_{em} = 400 nm, T = 37 °C. The signal of the equimolar solution of $^{th}\mathbf{G}_N$ is shown for reference.

with the known activity of O^6-(4-bromothenyl)guanine (Lomeguatrib, also known as PaTrin-2; cf. inset in Fig. 4b) to deactivate MGMT at a much higher rate than O^6-benzylguanine and its derivatives substituted in the phenyl ring.[31,32] Altogether, these data indicate that $^{th}\mathbf{G}_{th}$ and $^{th}\mathbf{G}_I$ can be used as probes for real-time monitoring of the MGMT activity.

Considering the fact that final fluorescence intensity linearly depends on the amount of formed $^{th}\mathbf{G}_N$ and is thus equivalent to the amount of added MGMT, our system may be useful for quantifying the amount of the active enzyme. In fact, precise quantification of MGMT activity is arduous since it requires [^{3}H]-

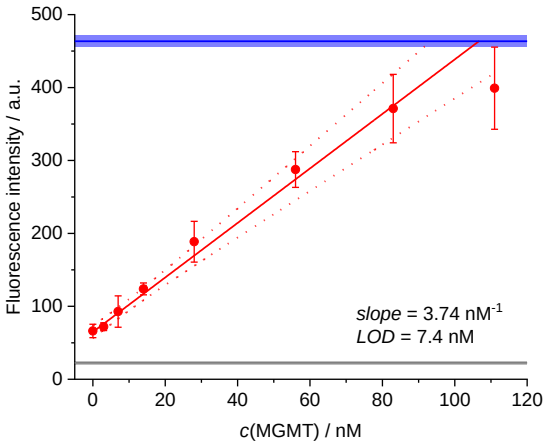

Fig. 3 Fluorescence intensity of $^{th}\mathbf{G}_{th}$ solutions (initial probe concentration: 100 nM in 10 mM Tris-HCl, 100 mM NaCl, 1 mM DTT, 5% v/v DMSO, pH 8.5; V = 400 µL) recorded at t = 1800 s following the addition of indicated amounts of MGMT (final concentration). Data (mean ± s.d., N = 4) were fitted to a linear model (solid red line) with 95% confidence intervals shown as red dotted lines. Fluorescence intensity (mean ± s.d., N = 4) of the equimolar $^{th}\mathbf{G}_N$ solution (blue line and shaded area) and the buffer (grey line and shaded area) are shown for comparison.

radiolabelled substrates that are not (or no longer) commercially available,[33,34] and the methods employing oligonucleotide substrates are biased due to multimerization of the enzyme in the presence of DNA, requiring excess of the protein for a complete conversion of the substrate.[35,36] Towards this end, we plotted fluorescence intensity of $^{th}\mathbf{G}_{th}$ solutions observed at t = 30 min after the addition of various amounts of MGMT. Linear response was observed in almost whole range of sub-stoichiometric MGMT concentration (Fig. 3), indicating that this stoichiometric reaction can be used for quantification of MGMT activity with a detection limit of 7.4 nM (corresponding to 3 pmol MGMT in our setup), which is comparable with other fluorescence-based methods for MGMT detection.[12,20,37]

Fluorimetric monitoring of MGMT activity may also be exploited for assessing the efficiency of MGMT inhibitors that represent potentially useful chemotherapeutic drugs.[38,39] As a proof-of-principle, we studied the fluorimetric response of $^{th}\mathbf{G}_{th}$ incubated in the presence of MGMT (110 nM, 1.1 molar equiv.) and various concentrations of Lomeguatrib, a reference MGMT inhibitor. In the presence of inhibitor, the final level of $^{th}\mathbf{G}_N$ fluorescence was clearly decreased, demonstrating the competition between Lomeguatrib and the probe for reaction with the enzyme (Fig. 4a). A sigmoidal dependence of the fluorescence intensity at t = 1000 s (or longer time points), converted into relative enzymatic activity, on the inhibitor concentration was observed, allowing to determine an IC_{50} value of 76 nM through fitting the experimental data to a logistic function (Fig. 4b).

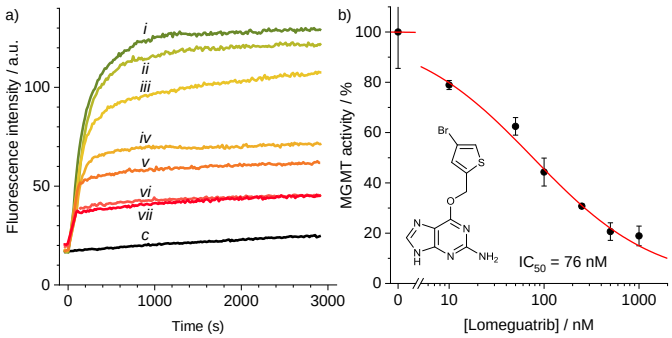

Fig. 4 a) Real-time fluorescence changes upon reaction of $^{th}G_{th}$ (100 nM) incubated in the absence (*c*) or in the presence (*i*–*vii*) of MGMT (110 nM) and increasing amounts of Lomeguatrib (final concentration, *i*: 0, *ii*: 10 nM, *iii*: 50 nM, *iv*: 100 nM, *v*: 250 nM, *vi*: 500 nM, *vii*: 1 μM). Buffer composition and experimental conditions as in Fig. 2 caption. b) Dose-response curve constructed by plotting relative MGMT activity (= [FI(*x*)–FI(*c*)]/[FI(*i*)–FI(*c*)] × 100% at *t* = 1000 s; *c* and *i* as in panel (a), *x* = *ii*–*vii*) vs. Lomeguatrib concentration and fitted to a logistic function with IC_{50} = 76 nM. Data are means ± s.d. from three independent experiments. Inset: structure of Lomeguatrib (a.k.a. PaTrin-2).

In summary, we designed first small-molecule chemosensors of MGMT, whose enzymatic dealkylation can be monitored in real time due to formation of the highly emissive thienoguanine. Interestingly, the fact that $^{th}G_{th}$ and $^{th}G_{I}$ are excellent MGMT pseudosubstrates is in line with the notion that the imidazole ring, and in particular the N7 atom of O^6-methylguanine and its analogues, do not form contacts with the active site and are not required for the reaction with the enzyme.[40] Due to the high fluorescence quantum yield of $^{th}G_{N}$, the chemosensors can be employed at concentrations as low as 100 nM (or lower with a more sensitive equipment) for monitoring MGMT activity, e.g., in cell extracts or tumour biopsies. It can also be applied for high-throughput screening of MGMT inhibitors and quantitative evaluation of their activity, as illustrated with an example of a previously reported inhibitor. Moreover, small molecular size (< 400 Da) and lipophilicity of $^{th}G_{I}$ and $^{th}G_{th}$ render these probes potentially live cell-permeant; unfortunately, poor brightness (1800 cm^{-1} M^{-1}) and UV absorption of $^{th}G_{N}$ reporter preclude their use in cell cultures at the current stage. These issues may be tacked in the future by the use of brighter, red-shifted fluorescent guanine analogues.[23,41]

This work was supported by the European Union's Horizon 2020 Framework Programme under the Marie Skłodowska-Curie Grant Agreement No. 666003 through an IC-3i international PhD programme (PhD fellowship to JFP). The authors thank Dr. Sophie Bombard (Institut Curie) for helpful discussions.

Notes and references

1 D. Fu, J. A. Calvo and L. D. Samson, *Nat. Rev. Cancer*, 2012, **12**, 104–120.
2 N. Tsao, O. D. Schärer and N. Mosammaparast, *Crit. Rev. Biochem. Mol. Biol.*, 2021, **56**, 125–136.
3 H. Erasimus, M. Gobin, S. Niclou and E. Van Dyck, *Mutat. Res. Mutat. Res.*, 2016, **769**, 19–35.
4 W. Wick, M. Weller, M. Van Den Bent, M. Sanson, M. Weiler, A. Von Deimling, C. Plass, M. Hegi, M. Platten and G. Reifenberger, *Nat. Rev. Neurol.*, 2014, **10**, 372–385.
5 M. Butler, L. Pongor, Y. T. Su, L. Xi, M. Raffeld, M. Quezado, J. Trepel, K. Aldape, Y. Pommier and J. Wu, *Trends in Cancer*, 2020, **6**, 380–391.
6 S. Brandner, A. McAleenan, C. Kelly, F. Spiga, H. Y. Cheng, S. Dawson, L. Schmidt, C. L. Faulkner, C. Wragg, S. Jefferies, J. P. T. Higgins and K. M. Kurian, *Neuro. Oncol.*, 2021, **23**, 1457–1469.
7 A. Mansouri, L. D. Hachem, S. Mansouri, F. Nassiri, N. J. Laperriere, D. Xia, N. I. Lindeman, P. Y. Wen, A. Chakravarti, M. P. Mehta, M. E. Hegi, R. Stupp, K. D. Aldape and G. Zadeh, *Neuro. Oncol.*, 2019, **21**, 167–178.
8 N. Sahara, R. Hartanto, N. Yoshuantari, K. Dananjoyo, I. Widodo, R. Malueka and E. Dwianingsih, *Asian Pacific J. Cancer Prev.*, 2021, **22**, 3803–3808.
9 G. Cabrini, E. Fabbri, C. Lo Nigro, M. C. Dechecchi and R. Gambari, *Int. J. Oncol.*, 2015, **47**, 417–428.
10 M. Wickström, C. Dyberg, J. Milosevic, C. Einvik, R. Calero, B. Sveinbjörnsson, E. Sandén, A. Darabi, P. Siesjö, M. Kool, P. Kogner, N. Baryawno and J. I. Johnsen, *Nat. Commun.*, 2015, **6**, 8904.
11 P. Wu, J. Cai, Q. Chen, B. Han, X. Meng, Y. Li, Z. Li, R. Wang, L. Lin, C. Duan, C. Kang and C. Jiang, *Nat. Commun.*, 2019, **10**, 2045.
12 M. Tintoré, S. Grijalvo, R. Eritja and C. Fàbrega, *Bioorg. Med. Chem. Lett.*, 2015, **25**, 5208–5211.
13 A. A. Beharry, Z. D. Nagel, L. D. Samson and E. T. K. Kool, *PLoS One*, 2016, **11**, 1–15.
14 M. Tintoré, A. Aviñó, F. M. Ruiz, R. Eritja and C. Fàbrega, *J. Nucleic Acids*, 2010, **2010**, 632041.
15 N. Farag, R. Mattossovich, R. Merlo, Ł. Nierzwicki, G. Palermo, A. Porchetta, G. Perugino and F. Ricci, *Angew. Chem. Int. Ed.*, 2021, **60**, 7283–7289.
16 X. Wang, X. Yi, Z. Huang, J. He, Z. Wu, X. Chu and J. Jiang, *Angew. Chem. Int. Ed.*, 2021, **60**, 19889–19896.
17 K. Stöhr, D. Siegberg, T. Ehrhard, K. Lymperopoulos, S. Öz, S. Schulmeister, A. C. Pfeifer, J. Bachmann, U. Klingmüller, V. Sourjik and D.-P. Herten, *Anal. Chem.*, 2010, **82**, 8186–8193.
18 X. Li, S. Qian, L. Zheng, B. Yang, Q. He and Y. Hu, *Org. Biomol. Chem.*, 2012, **10**, 3189–3191.
19 W.-Y. Lai and K.-T. Tan, *J. Chinese Chem. Soc.*, 2016, **63**, 688–693.
20 W.-T. Yu, T.-W. Wu, C.-L. Huang, I.-C. Chen and K.-T. Tan, *Chem. Sci.*, 2016, **7**, 301–307.
21 T. Komatsu, K. Johnsson, H. Okuno, H. Bito, T. Inoue, T. Nagano and Y. Urano, *J. Am. Chem. Soc.*, 2011, **133**, 6745–6751.
22 X. Sun, A. Zhang, B. Baker, L. Sun, A. Howard, J. Buswell, D. Maurel, A. Masharina, K. Johnsson, C. J. Noren, M. Q. Xu and I. R. Corrêa, *ChemBioChem*, 2011, **12**, 2217–2226.
23 W. Xu, K. M. Chan and E. T. Kool, *Nat. Chem.*, 2017, **9**, 1043–1055.
24 D. Dziuba, P. Didier, S. Ciaco, A. Barth, C. A. M. Seidel and Y. Mély, *Chem. Soc. Rev.*, 2021, **50**, 7062–7107.
25 D. Shin, R. W. Sinkeldam and Y. Tor, *J. Am. Chem. Soc.*, 2011, **133**, 14912–14915.
26 M. Sholokh, R. Sharma, D. Shin, R. Das, O. A. Zaporozhets, Y. Tor and Y. Mély, *J. Am. Chem. Soc.*, 2015, **137**, 3185–3188.
27 Y. Mély, J. Kuchlyan, L. Martinez-Fernandez, M. Mori, K. Gavvala, S. Ciaco, C. Boudier, L. Richert, P. Didier, Y. Tor and R. Improta, *J. Am. Chem. Soc.*, 2020, **142**, 16999–17014.
28 P. Didier, J. Kuchlyan, L. Martinez-Fernandez, P. Gosset, J. Leónard, Y. Tor, R. Improta and Y. Mély, *Phys. Chem. Chem. Phys.*, 2020, **22**, 7381–7391.
29 R. Schirrmacher, B. Wängler, E. Schirrmacher, T. August and F. Rösch, *Synthesis*, 2002, 538–542.

30 M. Sholokh, R. Improta, M. Mori, R. Sharma, C. Kenfack, D. Shin, K. Voltz, R. H. Stote, O. A. Zaporozhets, M. Botta, Y. Tor and Y. Mély, *Angew. Chem. Int. Ed.*, 2016, **55**, 7974–7978.
31 J. Reinhard, W. E. Hull, C.-W. von der Lieth, U. Eichhorn, H. Kliem, B. Kaina and M. Wiessler, *J. Med. Chem.*, 2001, **44**, 4050–4061.
32 B. Kaina, U. Mühlhausen, A. Piee-Staffa, M. Christmann, R. G. Boy, F. Rösch and R. Schirrmacher, *J. Pharmacol. Exp. Ther.*, 2004, **311**, 585–593.
33 A. J. Watson and G. P. Margison, in *DNA Repair Protocols*, Humana Press, New Jersey, Vaughan, P., 2000, vol. 152, pp. 49–61.
34 K. Ishiguro, K. Shyam, P. G. Penketh and A. C. Sartorelli, *Anal. Biochem.*, 2008, **383**, 44–51.
35 H. Zang, Q. Fang, A. E. Pegg and F. P. Guengerich, *J. Biol. Chem.*, 2005, **280**, 30873–30881.
36 J. J. Rasimas, A. E. Pegg and M. G. Fried, *J. Biol. Chem.*, 2003, **278**, 7973–7980.
37 A. Hongo, R. Gu, M. Suzuki, N. Nemoto and K. Nishigaki, *Anal. Biochem.*, 2015, **480**, 82–84.
38 C. H. Fan, W. L. Liu, H. Cao, C. Wen, L. Chen and G. Jiang, *Cell Death Dis.*, 2013, **4**, e876-8.
39 G. Sun, L. Zhao, R. Zhong and Y. Peng, *Future Med. Chem.*, 2018, **10**, 1971–1996.
40 M. Y. Chae, K. Swenn, S. Kanugula, M. E. Dolan, A. E. Pegg and R. C. Moschel, *J. Med. Chem.*, 1995, **38**, 359–365.
41 Y. Saito and R. H. E. Hudson, *J. Photochem. Photobiol. C Photochem. Rev.*, 2018, **36**, 48–73.

Graphical abstract

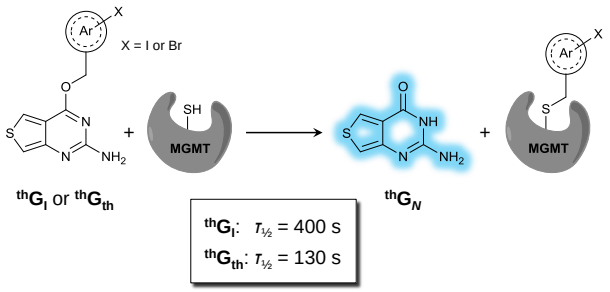

TOC entry: Activity of O^6-methylguanine-DNA-methyltransferase (MGMT) can be monitored in real time using chemosensors that generate an emissive guanine analogue, $^{th}\mathbf{G}_N$.